

Causal Effect Estimation with Global Probabilistic Forecasting: A Case Study of the Impact of Covid-19 Lockdowns on Energy Demand

Ankitha Nandipura Prasanna*, Priscila Grecov*, Angela Dieyu Weng†, and Christoph Bergmeir*

*Department of Data Science and Artificial Intelligence, Monash University, Melbourne, Australia.

†Lauriston Girls’ School, Melbourne, Australia

arXiv:2209.08885v1 [cs.LG] 19 Sep 2022

Abstract—The electricity industry is heavily implementing smart grid technologies to improve reliability, availability, security, and efficiency. This implementation needs technological advancements, the development of standards and regulations, as well as testing and planning. Smart grid load forecasting and management are critical for reducing demand volatility and improving the market mechanism that connects generators, distributors, and retailers. During policy implementations or external interventions, it is necessary to analyse the uncertainty of their impact on the electricity demand to enable a more accurate response of the system to fluctuating demand. This paper analyses the uncertainties of external intervention impacts on electricity demand. It implements a framework that combines probabilistic and global forecasting models using a deep learning approach to estimate the causal impact distribution of an intervention. The causal effect is assessed by predicting the counterfactual distribution outcome for the affected instances and then contrasting it to the real outcomes. We consider the impact of Covid-19 lockdowns on energy usage as a case study to evaluate the non-uniform effect of this intervention on the electricity demand distribution. We could show that during the initial lockdowns in Australia and some European countries, there was often a more significant decrease in the troughs than in the peaks, while the mean remained almost unaffected.

Index Terms—Smart grid, uncertainty, causal effect, energy demand forecasting, Covid-19 impact, probabilistic forecasting, global time series forecasting, counterfactual analysis, neural networks.

I. INTRODUCTION

The rise in global energy scarcity, energy efficiency and grid balancing issues have prompted many countries around the world to use intelligent energy management systems. In these smart grids, typically energy flow is bidirectional and distributed across multiple energy resources. A major challenge in such grids is to balance energy generation and consumption, due to the uncertainty caused by seasonality, natural disasters, technological advances, weather, and temperature [1], in both the generation and the consumption side. On the supply side, energy generated by renewable energy resources such as rooftop photovoltaics, wind power, and solar power can exacerbate network issues such as voltage control, loss and congestion in the network.

On the demand side, flexible demand from electric vehicles, energy storages, commercial and household consumption needs to be met on a regular basis by the electricity supply,

which requires planning and communication between both sides of the power system, i.e., generation and consumption. In particular, the supply-demand balance must be maintained to avoid system instability, power interruptions, and frequency deviations that are harmful to end-user appliances [2]. Thus, electric utilities must quantify the potential uncertainties associated with future generation and customer demand [3].

Forecasting methods, in particular probabilistic forecasting algorithms are commonly the tools of choice in this space. Research in this space has been driven by the GEFcom competition series (2012, 2014, and 2017) [4, 5], and there is now a rich literature in forecasting the energy supply and demand; especially also probabilistic approaches of forecasting the energy supply and demand have been proposed [6, 7, 8].

There are many external factors that influence both energy supply and demand, such as weather characteristics (wind speed and direction, solar irradiation, temperature), results of climate change such as natural disasters, or external shocks such as the Covid-19 pandemic. While forecasting methods can try to incorporate such external factors to achieve higher forecasting accuracy, policy makers and market participants often need to assess the impact of such external shocks to the energy market, need to consider different scenarios, and need to make decisions and assess the impact of these decisions.

This is the related domain of causal effect analysis methods. Causal effect analysis is the process of determining the effect of interventions, from which it enables to directly determine how, e.g., the changes in policy create changes in real world outcomes. This is accomplished by forecasting the counterfactual outcomes for affected instances and comparing them with the real outcomes. As effects of these interventions in the real world can be complex, it may often not be enough to look at their average effects. Instead, we want to assess how interventions or policy implementations affect the distribution of energy profiles in quantile levels. For example, an intervention may lead to higher minimal or maximal energy production/consumption, without altering the mean production/consumption.

To the best of our knowledge, very little research has been done in this area, so that our work is the first to take advantage of the recent and emerging literature on the use of machine learning (ML) techniques and probabilistic global forecasting methods (GFM), to construct counterfactual energy consump-

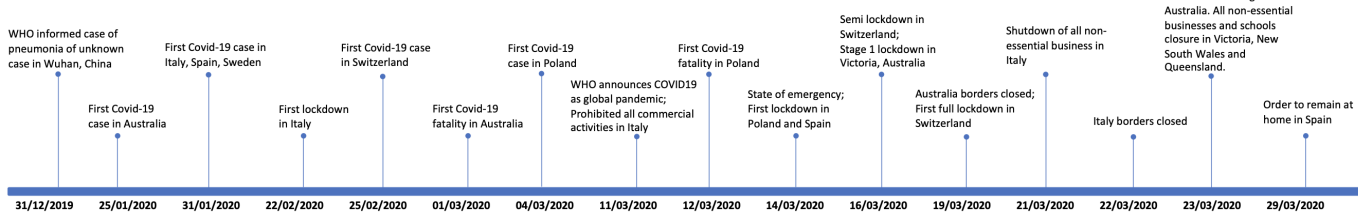


Fig. 1. Timeline of first lockdown in Australia and European countries.

tion paths and distributions after interventions. More recently, ML and probabilistic GFM approaches have provided important new tools to improve the estimation of causal effects from observational data in high-dimensional settings. Therefore, its application for causal effect analysis in the energy market enables flexible control of the usual high-frequency time series data in electricity markets. The hourly electricity consumption data allows us to incorporate a rich set of controls and fixed effects in order to non-parametrically separate the causal effect of a specific intervention from other confounding factors. When we train these ML-GFM models on pre-treatment data and use them to forecast counterfactual energy consumption paths and distributions without any intervention, it enables us to create flexible and data-driven models of energy use with less risk of overfitting that captures non-uniform effects over the demand distribution. Consequently, we can achieve more reliable treatment effect estimations. As far as we are aware, this paper provides the first empirical implementation of a neural network (NN) and probabilistic GFM framework for causal effect analysis in electricity markets.

An obvious case study to showcase our methodology is the Covid-19 pandemic and its associated lockdowns, which caused changes in lifestyle, closures of commercial buildings, schools, and whole business sectors. The International Energy Agency (IEA) indicated that the change in energy demand due to the pandemic is the largest in the last 70 years [9]. The change in lifestyle and work from home caused changes in daily demand distributions, e.g., in the form of a reduced shift in distribution, change in peak and troughs of the distribution. Those are crucial information for grid balancing [10, 11, 12].

The global rate of reduction in energy demand due to the pandemic ranges from 2% (mild impact) to 26% (extreme impact) [13]. Due to surplus energy generation, the reduction in energy demand causes voltage increase issues in some distribution systems, particularly in areas with many factories and commercial buildings that were fully or partially closed during Covid-19 lockdowns. Uncertainties in demand and generation further threaten the power balance.

In particular, we choose Australia and Europe as the regions to study the lockdown impact on energy consumption in our case study. This is because, firstly, they imposed restrictive lockdown measures at the very beginning of the pandemic at similar starting dates. Secondly, there are distinctions in how they established lockdown restrictions across the countries/states, with some regions not imposing them, which is essential for a causal impact analysis of policy interventions.

In detail, each state government in Australia imposed Covid-

19 restrictions in their respective timelines, causing a nationwide lockdown to begin on March 23, 2020; by this date, all non-essential businesses and schools in Australia were closed. Whereas in Europe, Italy was the first country that was hit severely and quickly by Covid-19. Spain and Poland went into lockdown on March 14, 2020, and Switzerland on March 16, 2020 (Figure 1). The pandemic resulted in the closure of all schools, commercial activities, and businesses, decreasing total country energy consumption. Because of the global decline in electricity demand, some electricity companies have been forced to reduce working hours in both the mining and generation segments, such as Tauron, one of Poland's largest electricity companies. It has consequently resulted in a global GDP drop [14].

We calculate the effect of the lockdowns as an intervention on each state in the Australian national energy market, and the effect of an intervention on countries across Europe per quantile to determine which quantile has the highest concentration of intervention impacts. We find that overall there is (unsurprisingly) a reduced energy consumption in Australian states and European countries. However, while some states or countries experienced a uniform consumption reduction, others experienced a non-uniform reduction or even some increases for specific parts of the energy demand distribution.

The rest of this article is organised as follows. In Section II, we discuss the prior work. In Section III, we present the architecture of our framework. In Section IV, we describe the context of the data and an empirical exercise over a real-world dataset. In Section V, we analyse the results obtained from the experiments and discuss the main insights resulting from them. Finally, Section VI concludes this work.

II. RELATED WORK

In the following, we revisit relevant background literature from the probabilistic forecasting and causal inference fields, as well as the primary literature that analyses the Covid-19 impact on energy demand.

A. Global probabilistic forecasting and causal inference

Early works that train models across series are Bandara et al. [15], Salinas et al. [6], Wen et al. [16]. However, such models have gained wider attention after such a cross-series model won the M4 forecasting competition [17], and have recently in the M5 competition [18] again shown that they are in many situations superior to models that are trained on each series separately. The terminology of global models

for forecasting was introduced by Januschowski et al. [19]. Those authors differentiated the methods that estimate the parameters independently for each time series (local models) and across all the time series available (global models). Both global and local models can be univariate or multivariate, where we focus on univariate versions that operate on one series at a time. Since GFMs benefit from training across multiple time series fitting a single model, they can often learn better the key patterns available across a collection of time series. Consequently, they often deliver more accurate forecasts [20, 21].

Probabilistic forecasting means the forecasting of future values in the form of a probabilistic forecast distribution, which gives insights into the uncertainty of the forecasts. The probabilistic forecasting method aims to maximise the sharpness of the forecast distribution based on the large set of historical data.

Salinas et al. [6] proposed DeepAR, which is arguably the most prominent model that enables global probabilistic forecasting. It performs probabilistic forecasting by predicting the parameters of a parametric forecasting distribution, such as negative binomial or Gaussian distributions. It is based on training an autoregressive Recurrent Neural Network (RNN) model on a large set of related time series, with special treatments when magnitudes in the series vary. RNNs process the data with temporal dependencies and carry that information (model parameters) across multiple time steps. The unfolded RNN can observe the model parameters from each time step and provide them to successive time steps. The gradient vanishing and exploding problems of RNNs are handled using the Long Short-Term Memory (LSTM) architecture. This model learns the temporal dependencies, seasonal patterns and trends to forecast the full probability distribution of the forecast.

On the other hand, causal inference refers to the process of drawing a conclusion that a specific treatment or intervention was the “cause” of the effect or observed outcome. The main goal of the causal inference literature is to find the impact of an intervention which is vital during policy making. Causal effect estimation is the difference between the counterfactual outcome (prediction in the absence of intervention) and actual post-intervention observation. The non-parametric nature of counterfactual prediction models overcomes the issue of parametric modelling and limitations of structural causal models [22]. The transition from local to global models (considering all the available time series) led to considerable advances in the forecasting domain that yet have to be fully reflected in the causal inference literature. The only works we are aware of in this space, which we leverage in our work, are the works of Grecov et al. [22] and Grecov et al. [23]. Grecov et al. [22] introduced the DeepCPNet, using a globally trained RNN for counterfactual prediction, in which the risk of bias in results is reduced by pre-splitting the data, and LSTM cells are used to avoid gradient vanishing or exploding problems. Grecov et al. [23] introduced a probabilistic version of the former method, which we extend in our work, e.g., by using a parametric approach to probabilistic forecasting.

We observe that the benefit of state-of-the-art methods of probabilistic forecasting, global forecasting and synthetic

control methods has not been unlocked yet for causal inference in the electricity domain. Motivated by this gap, we propose a practical framework that combines global and probabilistic forecasting methods by employing DeepAR to generate counterfactual predictions to estimate the impact caused by Covid-19 on energy consumption.

B. Covid-19 impact analysis on energy demand using machine learning models

Kwekha-Rashid et al. [24] conducted an experimental study to analyse the machine learning applications used in Covid-19 disease, with Logistic Regression being the most commonly used machine learning algorithm. Many works in the literature to analysing the impact of Covid-19 on energy demand are completed through exploratory data analysis and the use of several analytical tools to present the energy usage, peak demands, and demand profiles visually, and compare the various countries around the world with their energy consumption. There are various machine learning and statistical models that are implemented in the literature to evaluate the impact of Covid-19 on electricity markets, such as, linear regression [13, 25], ARIMA [14], Artificial Neural Networks [26], probabilistic forecasting models [27], clustering [28, 13, 26] and counterfactual prediction [29, 30] to analyse the impact.

The unified modelling framework proposed by Buechler et al. [13] explores the relationship between change in electricity demand, mobility and government restrictions. This method estimates the region-specific regression models to predict electricity consumption without the pandemic accounting for weather, seasonal and temporal effects and further K-Means clustering is applied to investigate the similarity in the response between different countries. Liu et al. [28] used Gaussian mixture modelling to analyse the demand data to identify the demand profile based on the typical magnitude of energy use, the timing of peak demands and shapes of energy use patterns.

In addition, the impact of the Covid-19 pandemic on gaseous and solid air pollutants is estimated using ARIMA model by Rybak and Rybak [14]. The K-Means algorithm has been implemented by García et al. [31] to perform automatic customer clustering to split the residential and non-residential customers based on the behaviour during the pandemic. Burlig et al. [32] generated the counterfactual outcome with the Lasso regression model for analysing the energy efficiency, then comparing the predicted outcome to the realised outcome to calculate the treatment effect. Graf et al. [30] proposed a counterfactual neural network model to predict business-as-usual re-dispatch costs in the electricity market and compare them to actual re-dispatch costs for the pre-covid and Covid-19 lockdown periods. Abrell et al. [29] estimated the impact intervention using the prediction-based estimator. This treatment effect estimator is based on counterfactual outcome and accounts for the influence of observed and unobserved variables.

In comparison, probabilistic forecasting is used in only a few papers in the electricity literature to assess the impact of the pandemic. Van der Meer et al. [27] used Gaussian

processes (GPs) as a non-parametric model to generate probabilistic forecasts of electricity consumption, photovoltaic (PV) power generation and net demand. This framework includes both a direct and an indirect method of evaluating net demand using static and dynamic GPs, with the dynamic GPs producing sharper prediction intervals while requiring less computational effort.

C. Energy demand changes in Australia and European countries due to the Covid-19 crisis

Several studies have been conducted to analyse the energy demand data of many countries around the world, considering the behaviour of the level of restrictions imposed. Beck and Hensher [33] conducted a survey in the middle of March 2020 to measure the people's attitude on changes in travel activity due to lockdown. The comparison of Melbourne and Sydney CityMapper Mobility Index curves begins to fall precipitously during the lockdown, with weekly household trips dropping by half. The aviation industry took a significant hit due to the border closure in Australia, with 47% of passengers cancelling their flights. PERCY and Mountain [34] conducted a descriptive analysis of the percentage change in average weekly electricity demand in selected Australian states, which revealed the greatest demand reduction in New South Wales, almost no change in Queensland and Victoria, and a slight increase in Tasmania and South Australia.

Furthermore, the EU's energy consumption fell by around -12.6%. Italy was the first country to be hit by the pandemic, and by the end of February, it had imposed lockdown measures. Italy is a highly informative case study due to the short-term economic impact of gradually increasing the severity of restrictions and the possible path for economic recovery. According to Bompard et al. [35], the demand reductions in Italy, Spain, Poland, Switzerland, and Sweden are -20.9%, -16.9%, -6.5%, +0.3%, and -0.3%, respectively. Sweden's average daily load profile (ADLP) is relatively close to 2019 and 2020 and has never imposed/milder confinement restrictions. The economic impact of the Swedish measures is less severe than seen elsewhere. Sweden is consensus-driven [36], where there are cooperations between the state and its citizenry, and it is also referred to as a society of state individualism. However, Poland has been grappling with the issue of rising energy demand [37], necessitating electricity imports. Reduced energy consumption did not result in lower energy imports in Poland, causing the country's economy to slow. Whereas Switzerland has 26 cantons, each canton experienced a wide range of reductions ranging from extreme reduction to mild reduction [25].

Finally, the previously described cutting-edge methods for analysing the impact of Covid-19 on energy sectors in the electricity literature are primarily focused on visualising and analysing the change in demand using simple statistical tools. Furthermore, the use of ML methods is limited to predicting post-pandemic data, which is done by using local models and comparing them to actual data. Even when GFM are used, the average energy consumption is examined [27], but not the distribution's quantile levels. The state-of-the-art methods in

the smart grid literature, probabilistic forecasting [38, 39, 40], and quantile regression [41] were implemented to understand the uncertainty and volatility in future demand to construct reliable and energy efficient smart grids. But the quantile level analysis of the energy demand distribution is critical for understanding the distribution's peaks and troughs and must be accurate to provide an efficient decision support. The increase or decrease in demand can be observed by examining the behaviour of the impact using the various forecasted quantiles. To fill this gap, this study employs a probabilistic forecasting approach to assess the impact of the pandemic by each quantile of the electricity demand.

III. METHODOLOGY

In the following, we first define the basic setup of counterfactual and causal effect estimation problems for counterfactual and synthetic control methods. Second, we introduce the neural network global forecasting engine used to generate the counterfactual point predictions. We close the section by presenting the incorporation of the quantile probabilistic technique into the previous method to forecast the counterfactual full distribution.

A. The Basic Setup of the Counterfactual and Causal Effect Estimation Problem

Let us consider a set of n time series units (countries, states, municipalities, firms, etc.) indexed by $j = 1, \dots, n$. For each unit and for every time period $t = 1, \dots, T$, we observe a realisation of a variable Y_{jt} . Furthermore, we assume an intervention (treatment) took place at $T_0 + 1$, where $1 < T_0 < T$, over only a subset i of *treated* units, where $i < n$. The remaining $c = n - i$ units, which we call *control* units, are never affected by this intervention for all t .

In addition, consider $\mathcal{D}_t \in (0, 1)$ be a binary variable that flags the periods where intervention was in place (binary treatment). That means $\mathcal{D}_t = 1$ when $t > T_0$, and $\mathcal{D}_t = 0$ otherwise. Therefore, following the potential outcome notation, we can express $Y_{i,t}$ such that:

$$Y_{i,t} = \mathcal{D}_t Y_{i,t}^{(1)} + (1 - \mathcal{D}_t) Y_{i,t}^{(0)}, \quad (1)$$

where $Y_{i,t}^{(1)}$ denotes the potential outcome when the treated unit i is exposed to the intervention, whilst $Y_{i,t}^{(0)}$ is the potential outcome when i is not exposed to the intervention (the counterfactual outcome). Moreover, under the synthetic control method (SCM) approach, we assume the control units $Y_{c,t}$ are independent of \mathcal{D}_t (unaffected by the treatment at any time) which means their observed outcomes are equal to their outcomes in the absence of the intervention, that is, $Y_{c,t}^{(1)} = Y_{c,t}^{(0)}$ for all $1 \leq t \leq T$.

Hence, the treatment effect estimation becomes the application of a forecast model \mathcal{M} to generate mean-unbiased proxies for the counterfactual of the i treated units, $P_{i,t}^{(0)} := \mathcal{M}(Y_{j,t \leq T_0}^{(0)}; \theta)$, where $\mathcal{M} : \mathcal{Z} \times \Theta \rightarrow \mathcal{Y}$ represents a general mapping function taking into account all true pre-intervention time series values $Y_{j,t \leq T_0}^{(0)} \in \mathcal{Z} \subseteq \mathbb{R}^d$ ($d > 0$) as covariates,

and model parameters $\theta \in \Theta$ of a finite-dimensional parametric space as follows:

$$Y_{i,t>T_0}^{(0)} = P_{i,t>T_0}^{(0)} + u_t, \quad E(u_t) = 0, \quad t = 1, \dots, T_0, \dots, T; \quad (2)$$

which under the assumption of stationarity on $Y_{j,t \leq T_0}^{(0)}$, u_t as an iid stationary stochastic process, and the knowledge of the exact start timing of a well-defined intervention, leads us to identify the treatment effect δ of a policy in period t as:

$$\hat{\delta}_t := Y_{i,t>T_0}^{(1)} - Y_{i,t>T_0}^{(0)}. \quad (3)$$

Consequently, the estimation of the *average treatment effect* (ATE) on the treated units over the post-treatment period can be represented by

$$\hat{\Delta}_T = \frac{1}{T - T_0} \sum_{t=T_0+1}^T \hat{\delta}_t. \quad (4)$$

In summary, the SCM requires the choice of a model $\mathcal{M}(\cdot, \cdot)$ which captures the information from the treated and control units using their pre-intervention data, which means that the counterfactual prediction is built considering a model trained in the absence of the intervention. Instead of using classical econometric causal models such as difference-in-difference (DiD) [42], SCM [43], penalised and constrained regression estimators [44], or Bayesian time series models [45], we propose the use of a more flexible model without the strong structural causal model assumptions. Applying RNNs for autoregressive time series forecasting in the context of the GFM approach, combined with quantile probabilistic forecasting techniques, we can estimate the counterfactual distribution as an outcome instead of only the counterfactual forecasting point estimation, as we detail in the following section.

B. Global Probabilistic Forecast Framework

1) *Neural Network Global Forecasting of Counterfactual Point Estimation:* Following the potential outcome framework [46], we aim to infer counterfactual outcomes $Y_{i,t}^{(0)}$ based on pre-treatment outcomes and covariates to estimate $\hat{\Delta}_t$ as defined in (4). Therefore, we train a NN model on an entire time series set of treated and untreated series groups (improving the basis for learning), which predicts outcomes after the policy intervention but under the unobserved effect of the treatment. The application of NN techniques enables the development of nonparametric predictors and thus the nonparametric identification of treatment effects, capable of capturing non-linear correlations across the historical values. In the context of our experimental study, we use only the data before the mandatory Covid-19-related lockdowns to train the model. Thus, in the absence of other confounding factors, the difference between our predicted counterfactual energy consumption and our factual data on electricity use after the advent of Covid-19 will be the causal impact of lockdown restrictions on electricity consumption.

The framework we propose follows the idea introduced by [22, 23], where the non-linear mapping \mathcal{M} is a GFM-RNN

forecast modelling to generate mean-unbiased counterfactual proxies, $P_{i,t}^{(0)}$. The idea is to fit a forecasting method based on autoregressive RNNs, which learns a *global* model from historical data of all time series in the dataset jointly. Hence, the *global* modelling approach allows the $P_{i,t}^{(0)}$ to be estimated considering both treated and control time series in the pre-treatment data, $Y_{i,t \leq T_0}$ and $Y_{c,t \leq T_0}$, as input variables to train the model – the covariates. Therefore, Equation (2) can be re-written as

$$Y_{i,t>T_0}^{(0)} = \mathcal{M}(Y_{j,t \leq T_0}, \theta) + u_t. \quad (5)$$

Whereas with the post-treatment prediction for the treated units $Y_{i,t}^{(0)}$ we reach the counterfactual outcomes; on the other hand, the assumption of null intervention effect over the controls $Y_{c,t}$, added to the *global* modelling with shared parameters θ across all series j , enables the post-treatment prediction of $Y_{c,t}$ to serve as a check of the forecast quality in the post-treatment period $t > T_0$. The parameter θ is estimated in the pre-treatment period and is used for predicting the control and treated time series. Therefore, when we implicitly test for the null effect over the controls, this is a test of how well the model parameters perform in the post-treatment period.

The choice of the GFM-RNN modelling in our work is based on the approach established in the literature by Salinas et al. [6] by using an autoregressive RNN global time series model called DeepAR, which is available on the GluonTS¹ library, a Python library for deep-learning-based time series modelling [47]. DeepAR is a global sequence-to-sequence (Seq2Seq) neural net and parametric probabilistic forecasting model mainly used for non-linear and non-stationary time series forecasting. In our implementation, DeepAR consists of an RNN (using LSTM cells) that takes the previous time points of related time series and covariate time series as inputs, learning a global model from the history of all sets of time series jointly. Thus, given the J treated and control univariate time series $\{y_{j,1:T_0}\}_{j=1}^J$, the objective of our neural network is to model the future trajectories of each time series $\{y_{j,T_0+1:T}\}_{j=1}^J$ after the intervention given its past pre-intervention data (in the absence of the intervention), which are the inputs/covariates of our global network as follows:

$$\{y_{j,T_0+1:T}\}_{j=1}^J = m_G(y_{:j,1:T_0}, \Theta), \quad (6)$$

where m_G denotes our GFM-DeepAR model, Θ denotes the set of learnable parameters of the network model, and $y_{j,t} \in \mathbb{R}$ is the value of the j -th time series at time t .

The pre-intervention time series $y_{j,t}$ are provided to an autoregressive LSTM whose architecture follows that described by Salinas et al. [6]. This LSTM is autoregressive and recurrent in the sense that it takes as inputs the values of the previous time step ($y_{:j,t-1}$) and the previous hidden state of the network ($h_{j,t-1}$). Hence, this autoregressive LSTM of $m_G(\cdot)$ model can be expressed in terms of its hidden states (h_t) as follows:

$$\mathbf{h}_{j,t} = r(\mathbf{h}_{j,t-1}, y_{:j,t-1}, \Theta), \quad (7)$$

¹<https://gluon-ts.mxnet.io>

where the function $r(\cdot)$ is a multi-layer RNN with LSTM cells parameterized by Θ .

The hidden state activation function in Equation (7) is a non-linear function such as the rectified linear unit (ReLU) function. We train the LSTM on pre-treatment outcomes using multiple training instances, i.e., sliding windows with different starting points and a fixed size of 1.25 times the prediction length. This moving window procedure allows to augment the data used and to learn the behaviour of the “new” time series by considering all other available covariates. Because implementation follows the GFM, the set of parameters Θ is learned globally across all J time series and shared for each value of t , which adds much more information to our modelling, consequently improving the accuracy of our counterfactual forecasting. Another gain when employing a GFM is that, differently from the current structural causal models based on the SCM approach, it is not required to assume that the post-treatment relationship between the treated and control time series is the same as that mapped prior to the intervention to enable the application of the estimated parameters over the post-treatment predictor time series, and therefore allow for identification. We do not need to assume this strict dependence because our estimation process is based only on the pre-treatment data. Our GFM-DeepAR modelling employs the ADAM optimiser with two-layer LSTM cells with 25 RNN cells for each layer.

In the following section, we explain how we combine the probabilistic forecasting techniques to this GFM-DeepAR model to estimate the distribution of the counterfactual as an outcome.

2) Probabilistic Global Forecasting of Counterfactual Distribution: DeepAR is a methodology for producing accurate probabilistic forecasts based on training an autoregressive RNN model on a set of many related time series. It is trained with maximum likelihood estimation to output the distribution parameters and to provide probabilistic forecasts by applying sequential sampling. When we suggest applying this methodology to the counterfactual forecasting for causal effect estimation, we are able to generate the counterfactual distribution for the treated units in the absence of the intervention effects and, therefore, estimate the distribution of the treatment effect across the period of intervention. Such probabilistic estimations are crucial in many causal effect studies as, in contrast to point forecasts, they enable optimal decision-making under interventions that affect the distribution non-uniformly or when facing skewed distributions.

DeepAR either estimates parameters of a parametric distribution (such as Gaussian, Student’s t, gamma, and negative binomial) or a highly flexible parameterisation of the quantile function. The default distribution to evaluate the historical observations and generate the sample predictions (within the GluonTS library) is the Student’s t distribution, which is the one considered for the experiments in this paper. In our application, this probabilistic part of DeepAR has as its goal to model the conditional distribution of the post-intervention time series, i.e., $P(y_{j,T_0+1:T}|y_{j,1:T_0})$. As the model uses an autoregressive RNN architecture (as expressed by Equation (7)), the model distribution $L_\Theta(y_{j,T_0+1:T}|y_{j,1:T_0})$ consists of

a product of likelihood factors such as

$$\begin{aligned} L_\Theta(y_{j,T_0+1:T}|y_{j,1:T_0}) &= \prod_{t=T_0+1}^T L_\Theta(y_{j,t}|y_{j,1:t-1}) \\ &= \prod_{t=T_0+1}^T p(y_{j,t}|\theta(\mathbf{h}_{j,t}, \Theta)), \end{aligned} \quad (8)$$

parameterised by the output $\mathbf{h}_{j,t}$ of the autoregressive RNN. The likelihood $p(y_{j,t}|\theta(\mathbf{h}_{j,t}))$ is a fixed Student’s t distribution with parameters estimated by the function $\theta(\mathbf{h}_{j,t}, \Theta)$ of the LSTM output $\mathbf{h}_{j,t}$ (as defined in (7)).

From the final probabilistic forecasting of $\{y_{j,T_0+1:T}\}_{j=1}^J$, we extract a wide range of Q prescribed quantiles τ for all time series j . This full list of quantile forecasting is then assembled to build the estimated quantile Student’s t distribution, as follows

$$\begin{cases} (\hat{y}_{j,t+1}^{(\tau_1)}, \dots, \hat{y}_{j,t+K}^{(\tau_1)}) &= m_G(h_t, y_{j,:t}; \Theta)[\tau_1] \\ (\hat{y}_{j,t+1}^{(\tau_2)}, \dots, \hat{y}_{j,t+K}^{(\tau_2)}) &= m_G(h_t, y_{j,:t}; \Theta)[\tau_2] \\ \dots \\ (\hat{y}_{j,t+1}^{(\tau_Q)}, \dots, \hat{y}_{j,t+K}^{(\tau_Q)}) &= m_G(h_t, y_{j,:t}; \Theta)[\tau_Q] \end{cases}, \quad (9)$$

where $y_{j,:t}$ are all the j time series to forecast, m_G is our *global* LSTM with its parameters shared across all forecasting horizons $k \in \{1, \dots, K\}$ and unit time series $j \in \{1, \dots, J\}$, h_t are the hidden states of our LSTM where all history is encoded, $\tau_{(\cdot)}$ denotes each of the $q \in \{1, \dots, Q\}$ quantiles, and $y_{j,:t}$ are the temporal inputs/covariates available in the pre-intervention history (the $Y_{j,t \leq T_0}$).

The system in (9) can be simplified by $\hat{\mathbf{Y}} = m_G(h_t, y_{j,:t}; \Theta)$, where $\hat{\mathbf{Y}}_{i,:t}$ corresponds to the Q counterfactual quantile predictions for all treated units whereas $\hat{\mathbf{Y}}_{c,:t}$ are the Q quantile forecasts for all control units.

To build and plot the estimated quantile distribution function post-intervention against the domain $[0, 1]$ for each forecast time series j , we pass the series $\{\hat{y}_{j,t+k}^{(\tau_1)}, \dots, \hat{y}_{j,t+k}^{(\tau_Q)}\}$ through the quantile function $qt()$ of the Student’s t distribution in R, once the probabilistic forecasting was executed assuming this parametric distribution to generate the predictions.

Finally, considering these quantile forecasts, we can now contrast the quantile distribution of the factual data against the estimated quantile distribution of the counterfactual, post-intervention, and the causal effect identification estimated by Equation (3) now might be expressed for each quantile τ as

$$\hat{\delta}_t^{(\tau)} := \hat{Y}_{i,\tau}^{(1)} - \hat{Y}_{i,\tau}^{(0)}, \quad (10)$$

and the ATE for a specific quantile τ , or by considering the mean of all quantile effects together, respectively, as

$$\hat{\Delta}_T^{(\tau)} = \frac{1}{T - T_0} \sum_{t=T_0+1}^T \hat{\delta}_t^{(\tau)}, \quad (11)$$

$$\hat{\Delta}_T = \frac{1}{Q} \sum_{q=1}^Q \frac{1}{T - T_0} \sum_{t=T_0+1}^T \hat{\delta}_t^{(\tau_q)}. \quad (12)$$

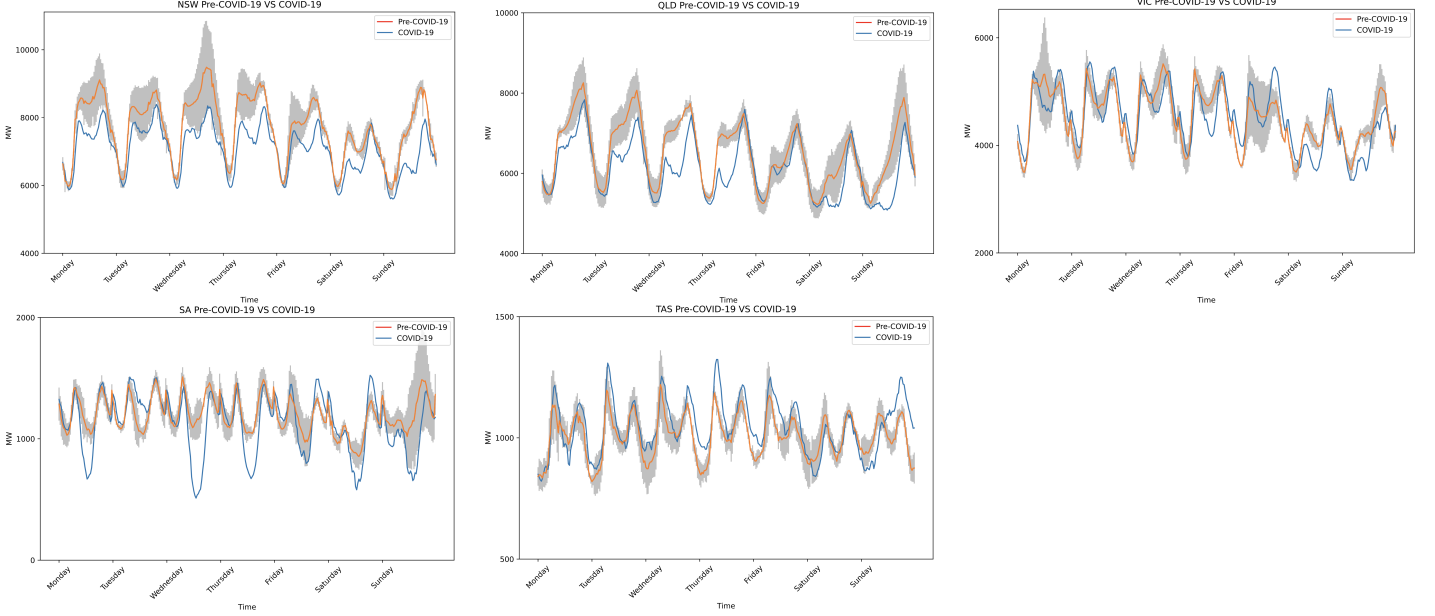


Fig. 2. The impact of Covid-19 on average weekly energy demand in the Australian states NSW, QLD, VIC, SA, and TAS.

IV. EXPERIMENTS

In this section, we first describe the context of the data collection process as the characteristics of the datasets to be analysed. Subsequently, we present an exploratory analysis of the data to select the time series that will be considered as treated and control units across the study. Then, we present the baseline models used to compare our method, the error metrics employed to evaluate the performance of the models, and finally, the hypothesis and placebo tests we perform.

A. Context and Data

We obtained data from two main sources. In particular, we analysed AEMO dataset [48] on electricity demand and the ENTSO-E Transparency Platform dataset [49] on European countries' total electricity load.

The AEMO dataset holds aggregated price and energy demand data across 5 of the 6 Australian states in 30-minute intervals. The entire data series are taken from January 2017 to April 2020. The observations from March 2020 to April 2020 are used as a test set because they correspond to the intervention period. The intervention period is determined by the presence of Covid-19 lockdowns to prevent the spread of the virus. The pre-intervention period is set in the absence of these measures, from January 2017 to February 2020.

The ENTSO-E dataset contains the total electricity load of 37 European countries in 1-hour intervals. Our data series are obtained from January 2016 to March 2020 in Italy, Poland, Spain, Switzerland and four bidding zones of Sweden. The test data is from the 16th of March 2020 to the 30th of March 2020, when all countries except Sweden imposed Covid-19 lockdowns to inhibit the virus propagation. Such as the Australian case, the pre-intervention period is determined when no lockdowns were imposed; thus, it is set from the 1st of January 2016 to the 15th of March 2020.

B. Exploratory Data Analysis

Figure 2 displays the differences between Australian states' mean weekly energy consumption pre-Covid-19 and during the pandemic. Our primary variable of interest is electricity consumption, observed at 30-minute intervals from 2017 to 2020. The pre-treatment weekly consumption was averaged from January 2017 to February 2020, whilst the post-intervention data was from March 2020. The standard deviation was measured for each data point and illustrated in grey.

From Figure 2, we observe an apparent reduction in energy demand in New South Wales (NSW) after the Covid-19 advent. The decrease in demand is most evident during working hours on weekdays, where there is a clear vertical downward shift of the morning and evening peaks. The exogenous shock likely causes this shift as the energy demand curve for post-Covid-19 is not within the standard deviation of pre-Covid-19 data. The weekday minima are relatively constant where energy demand for post-Covid-19 remained within the standard deviation, indicating that working from home is a plausible justification for such a trend. Greater fluctuations are evident for the weekend, where the figure showed a significant decrease in energy demand on Sunday, likely due to mandatory lockdowns. There is more significant variability in energy demand for Victoria (VIC) and South Australia (SA), with no clear differences in Tasmania's energy demand as no lockdown was imposed. Thus, the figure validates that Tasmania (TAS) should be used as a control unit for the Australian data set. The post-Covid-19 energy demand trend in Queensland (QLD) is atypical, significantly reducing the morning peak. We speculate that solar energy may have contributed to this phenomenon. The shape of Friday's energy demand is similar to Saturday's, which may be due to a behavioural change in energy usage approaching the weekend.

Figure 3 illustrates the differences between mean weekly

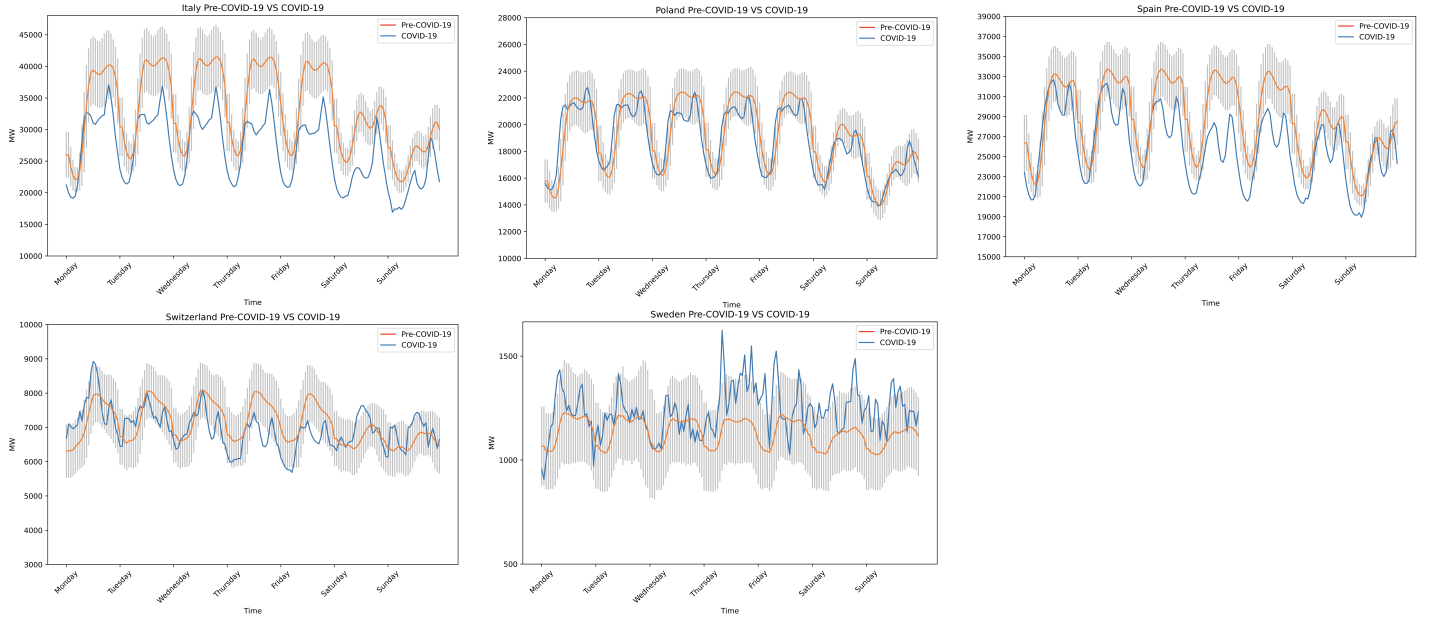


Fig. 3. The impact of Covid-19 on average weekly energy demand in Italy, Poland, Spain, Switzerland, and Sweden.

energy consumption pre-Covid-19 and post-Covid-19 in 5 European countries. The pre-Covid-19 data was averaged from January 2016 to early March 2020, whilst the post-intervention data was from the 16th to the 22nd of March. The standard deviation was computed for each data point and illustrated in grey to cater for variability.

We observe that the exogenous shock of Covid-19 reduces energy demand in Italy and Spain. The post-Covid-19 energy demand curve was vertically shifted downward, surpassing the lower boundaries of the standard deviation. The decrease in demand is most evident during maxima and minima. The evening peak of energy demand is relatively higher than the morning peak during the pandemic, which was not evident pre-Covid-19. This is likely due to the relatively lower energy usage in the morning, thus, magnifying the evening peak. An apparent reduction in energy demand is observable through preliminary descriptive data analysis. Similarly, Spain showcases an apparent reduction in energy demand. The most significant decrease is observed between the morning and evening peaks. This difference in the shape of pre-pandemic and during pandemic data for Spain and Italy will be further discussed later in the paper.

Both post-Covid-19 data for Switzerland and Poland are within the standard deviation. The higher variability may be due to the post-Covid-19 data being only a single week of data. There is some reduction in energy usage during daytime in Poland and a relatively more apparent decrease on Thursdays and Fridays in Switzerland. Behavioural changes during Covid-19 may be a possible justification. The relatively small reduction during daytime prompts to analyse quantiles.

Four bidding zone data was available for Sweden; however, considering the population density and initial quantile analysis, Sweden bidding zone 1 (Sweden1) was selected for the control unit as no lockdowns were imposed in Sweden. The post-

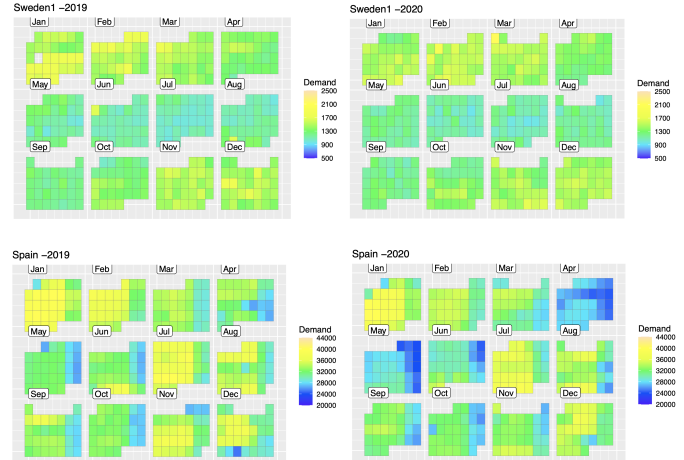


Fig. 4. Heat map of energy demand in Sweden1 and Spain for 2019 vs 2020

Covid-19 data for Sweden exhibited the most fluctuation; however, this could be justified due to the relatively small population. The variability is primarily within the standard deviation, validating Sweden as the control unit.

From Figure 4, the heat map graphs for Sweden1, comparing 2019 monthly energy demand to 2020 monthly energy demand illustrates the choice of it being the control unit. The graphs show minimal colour changes, thus energy demand across the consecutive years in contrast to other countries such as Spain in Figure 4. This, accompanied by the results from Figure 3, justifies Sweden1 as the control unit.

From Figure 4, the heat map graphs for Spain comparing 2019 monthly energy demand to 2020 monthly energy demand exhibit a significant reduction in energy usage from April to June, where the colour changes from light green and aqua to dark blue, indicative of a reduction of around 10,000MW.

It is speculated that the exogenous shock of Covid-19 likely contributed to this decrease. The heat map graphs support the results in Figure 3.

The data exploration clearly indicates the control unit in Australia and Europe and gives preliminary insights into the nuances of energy demand and expected results.

C. Baseline Models and Performance Measuring

We provide comparisons of the DeepAR against the following three baseline *local* time series forecasting models and two baseline *global* NN models, respectively:

- *Seasonal Naïve (local)*: a seasonal naïve forecaster where each forecast equals the last observed value from the same season. It was implemented using the `gluonts.model.seasonal_naive` package. The Seasonal Naïve model gives a naïve lower bound for forecasting performance that can be achieved.
- *ETS (local)*: the Exponential Smoothing (ETS) model (Hyndman et al. [50]) from the `forecast` R package. To forecast, ETS uses weighted averages of past observations, with the weights decaying exponentially as the observations go further back in time. We implement ETS using the wrapper `RForecastPredictor` from GluonTS which calls the R `forecast` package.
- *TBATS (local)*: the Trigonometric Box-Cox ARMA Trend Seasonal (TBATS) model, also from the `forecast` R package, uses an automated combination of Fourier terms with an exponential smoothing state space model and a Box-Cox transformation (De Livera et al. [51]). Identically to ETS, it was implemented by using `RForecastPredictor` from GluonTS.
- *FFNN (global)*: a global FFNN uses a simple multi-layer perceptron (MLP) model predicting the next target time steps given the previous ones. It was implemented using the `gluonts.model.simple_feedforward` package.
- *RNN (global)*: a canonical RNN model with LSTM as cell-type, which was implemented using the `model.canonical.CanonicalRNNEstimator` class in GluonTS.

Time series forecast evaluation is complex and not straightforward, and no generally accepted consensus exists in the field [52]. Common error metrics in the field, such as Mean Absolute Scaled Error (MASE) and symmetric Mean Absolute Percentage Error (sMAPE), have problems. For example, the sMAPE is not symmetric, and the MASE, though in general a good measure, has the problem that in our application we have a relatively large test set that we predict from a fixed origin. As such, if a one-step-ahead naïve forecast is used in the denominator in the MASE, the MASE is not easily interpretable in its typical way of values larger than 1 being bad forecasts. Instead, as our test sets are large, with their sums amounting to large values, we opt to use the Weighted Absolute Percentage Error (WAPE) and the Weighted Root Mean Square Percentage Error (WRMSPE) as two scale-independent forecast metrics that can be used to compare forecast performance between different time series [52]. They

are easily interpretable as percentages. Furthermore, we use the Mean Scaled Interval Score (MSIS) and the Continuous Ranked Probability Score (CRPS), which are probabilistic error metrics to evaluate probabilistic forecasting.

The metrics are defined as follows, and they are evaluated in the prediction range $h = T - T_0$, i.e., post-intervention:

$$WAPE = \frac{\sum_{t=n+1}^{n+h} |Y_t - \hat{Y}_t|}{\sum_{t=n+1}^{n+h} Y_t}, \quad (13a)$$

$$WRMSPE = \sqrt{\frac{\frac{1}{h} \sum_{t=n+1}^{n+h} (Y_t - \hat{Y}_t)^2}{\frac{1}{h} \sum_{t=n+1}^{n+h} Y_t}}, \quad (13b)$$

$$MSIS = \frac{1}{h} \left(\frac{\sum_{t=n+1}^{n+h} (U_t - L_t) + \frac{2}{\alpha} (L_t - Y_t) \mathbb{1}\{Y_t < L_t\} + \frac{2}{\alpha} (Y_t - U_t) \mathbb{1}\{Y_t > U_t\}}{\frac{1}{n-S} \sum_{t=S+1}^n |Y_t - Y_{t-S}|} \right), \quad (13c)$$

$$CRPS = \int_0^1 2\mathcal{L}_\tau(\widehat{CDF}^{-1}(\tau), z) d\tau. \quad (13d)$$

Here, Y_t and \hat{Y}_t are actuals and forecasts, respectively, n the in-sample size, L_t and U_t in (13c) are the lower and upper bounds of the corresponding prediction interval for period t , S the seasonal frequency, α defines the prediction interval (i.e., $\alpha = 0.05$ for a 95% interval), and $\mathbb{1}$ is the indicator function (being 1 if Y_t is within the postulated interval and 0 otherwise). Finally, in (13d) we have \widehat{CDF}^{-1} representing the quantile function (indicated by the inverse of the cumulative distribution function), and \mathcal{L}_τ the quantile loss which is expressed by $\mathcal{L}_\tau(Y_t, \hat{Y}_t) = \max[\tau(\hat{Y}_t - Y_t), (\tau-1)(\hat{Y}_t - Y_t)]$, where τ is a certain quantile of the predictive distribution. Lower values of MSIS and CRPS indicate better prediction intervals.

D. Placebo and Hypothesis Testing

The forecasting performance of the different algorithms is evaluated by point estimating the outcomes only for the control units. In the absence of true underlying effects (where we have unobserved true counterfactual outcomes to compare), this process allows us to establish a baseline of prediction errors for confidently assessing the treatment effect later. The errors for control units need to be low and statistically significantly different from the error gaps of the treated units (the placebo test). On the other hand, the error gap of the treated units, the causal effect, must be statistically significantly different from zero. Therefore, we conduct hypothesis testing using both non-parametric statistical Wilcoxon signed-rank and rank-sum tests, as implemented, respectively, in the functions `wilcoxon` and `ranksums` from the `scipy.stats` library [53] in Python. That means we are first testing if the distribution of the difference between forecasts and true values is symmetric at about zero, and second, whether these values in one sample (treated units) are likely to be larger than the values in the other sample (control units). Hence, for our study, the hypothesis of interest are

$$\begin{cases} H_0^{(1)} : \hat{\Delta}_T = 0 \text{ and } H_0^{(2)} : \hat{\Delta}_T^i = \hat{\Delta}_T^c \\ H_A^{(1)} : \hat{\Delta}_T \neq 0 \text{ and } H_A^{(2)} : \hat{\Delta}_T^i \neq \hat{\Delta}_T^c, \end{cases} \quad (14)$$

where $\hat{\Delta}$ is the ATE as defined in Equation (12), and i and c denote the treated and control units, respectively.

For the treated units, the rejection of $H_0^{(1)}$ provides significant evidence about the existence of non-empty policy impacts. On the other hand, for the control units, an acceptance of $H_0^{(1)}$ is the desired outcome, to confirm the null intervention effect over the control units – the placebo test. In other words, the placebo test is: when comparing the prediction errors of the estimator for treated units (treatment effect) against the prediction errors for control units (post-intervention outcomes for control units), the distribution of prediction errors for the treated units must be substantially larger (treatment effect different from zero) relative to the distribution of prediction errors for the control units in the donor pool (null effect). In addition, in $H_0^{(2)}$, we also test, by using the Wilcoxon rank-sum test, the statistical difference between the errors for treated and control units.

V. RESULTS

In the following we present the results for the two use cases of Europe and Australia.

A. European Data

As we face the absence of true underlying effects in the synthetic counterfactual approach, we first check the errors only of the control units (unaffected by the intervention) to establish a baseline of prediction errors. They are reported in Table I for the Sweden1 time series forecasting as the control group. As explained earlier in Section IV-B and depicted in Figure 5, Covid-19 should shallowly impact Sweden1's energy demand, in contrast to Italy where the impact of Covid-19 is likely spread throughout the demand distribution.

Table I shows that the TBATS model, which is a local model that uses exponential smoothing to forecast time series with complex seasonal patterns, is able to outperform all other models, in terms of point prediction accuracy. However, it struggles to retrieve the true quantile distribution due to its non-probabilistic approach, which is depicted by the very low accuracy of the quantile predictions. When forecasts are probabilistic and observations are deterministic, CRPS and MSIS are critical metrics for comparing forecasting model accuracy. In terms of the forecast distribution, both the probabilistic DeepAR and FFNN global models performed better in obtaining prediction intervals with lower MSIS and CRPS values, resulting in a superior probabilistic forecast for control series.

Further, we analyse the counterfactual forecasting results for treated units, focusing only on the comparison between DeepAR and TBATS, as the best probabilistic and non-probabilistic methods from the previous analysis (Table I). Figure 6a (right) demonstrates how well (taking Italy as example) our global probabilistic baseline DeepAR model captures the distribution patterns from the unaffected observed

TABLE I
ERROR METRIC RESULTS FOR THE CONTROL UNIT (SWEDEN1) OF THE EUROPEAN DATA.

METHOD	WAPE	WRMSPE	MSIS	CRPS
DeepAR	0.123	0.148	15.009	0.090
RNN	0.133	0.164	18.734	0.099
FFNN	0.136	0.172	14.967	0.095
Seasonal Naïve	0.098	0.131	56.588	0.098
ETS	0.092	0.134	41.824	0.168
TBATS	0.088	0.117	44.026	0.179

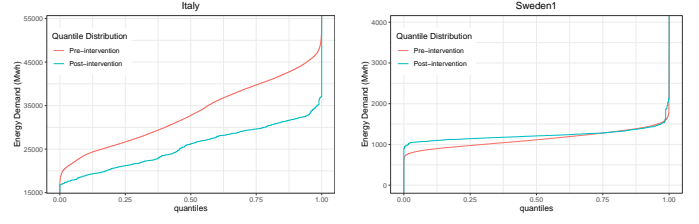


Fig. 5. Quantile distribution of observed pre- and post-intervention data of Italy and Sweden1.

data. We observe that the counterfactual distribution is more compatible with the pre-intervention data (without the effects of the lockdowns) but not the observed post-intervention data, confirming, therefore, the impact of lockdown measures on reducing the electricity demand. Point and distributional counterfactual estimations (left and right of Figure 6a, respectively) show this reduction, but the distributional forecast makes clearer the non-uniform aspect of this impact. Despite the counterfactual quantile function showing a decrease in demand spread across the entire distribution (right of Figure 6a), it evidences the stronger average effect in the troughs and the

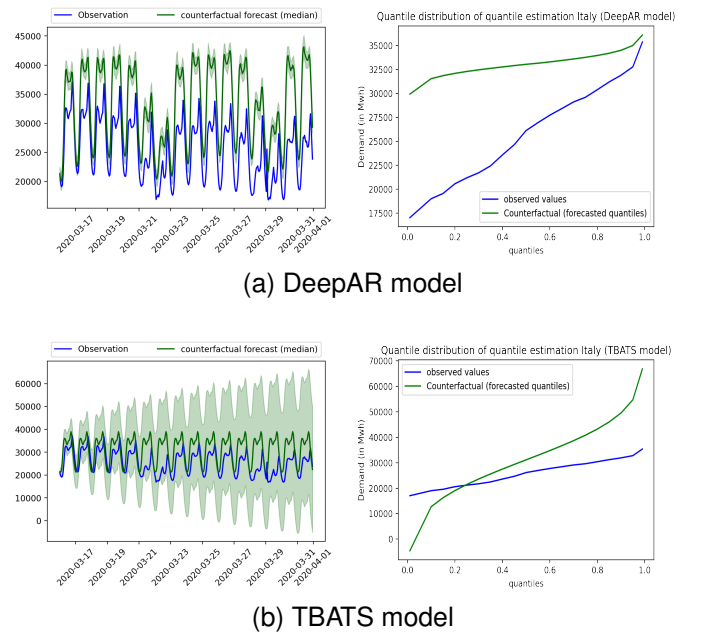


Fig. 6. Point counterfactual forecast of the DeepAR and TBATS model with 10% and 90% prediction interval (left) and the quantile distribution of the counterfactual forecast (right) for Italy.

TABLE II
AVERAGE CAUSAL EFFECT AND CHANGE IN ENERGY CONSUMPTION IN EUROPEAN DATA USING THE DEEPAR MODEL.

Quantiles	Italy		Poland		Spain		Switzerland		Sweden1	
	Avg. Causal Effect(in Mwh)	Change in Demand (%)	Avg. Causal Effect(in Mwh)	Change in Demand (%)	Avg. Causal Effect(in Mwh)	Change in Demand (%)	Avg. Causal Effect(in Mwh)	Change in Demand (%)	Avg. Causal Effect(in Mwh)	Change in Demand (%)
0.1	-12522.03	-65.84	-4574.77	-29.90	-7570.25	-36.59	-1273.93	-19.97	-145.62	-13.40
0.25	-11089.92	-52.31	-3993.76	-24.38	-6449.63	-28.72	-1218.97	-18.27	-148.15	-12.98
0.3	-10738.12	-49.43	-3860.16	-23.22	-5908.88	-25.52	-1206.36	-17.90	-148.51	-12.86
0.4	-9177.60	-38.92	-3104.13	-17.65	-4902.37	-20.06	-1079.43	-15.50	-144.71	-12.25
0.5	-6906.85	-26.43	-1985.74	-10.51	-3861.84	-15.01	-1087.14	-15.42	-136.31	-11.26
0.6	-5553.66	-20.03	-1134.97	-5.70	-3077.51	-11.51	-1022.09	-14.21	-133.74	-10.85
0.75	-4166.02	-14.08	-758.78	-3.68	-2059.89	-7.31	-926.34	-12.44	-122.12	-9.54
0.8	-3567.10	-11.74	-709.43	-3.41	-1680.12	-5.85	-934.04	-12.46	-104.76	-7.98
0.95	-2225.37	-6.79	-550.12	-2.54	-727.32	-2.38	-762.67	-9.53	-47.13	-3.24
0.99	-719.58	-2.03	-580.75	-2.60	-70.58	-0.22	-257.90	-2.91	282.12	15.07
p-values	4.7e-07 / 4.7e-07		0.005							

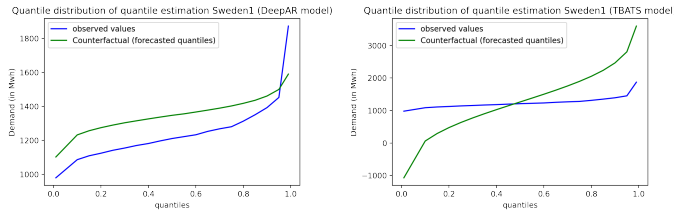


Fig. 7. Quantile distribution of the counterfactual forecast for Sweden1 using DeepAR (left) and TBATS (right) models.

less substantial impact over the peaks of demand. The fact that DeepAR's median forecast has remained in the centre of the model's prediction confidence intervals (left of Figure 6a), ensures the quality of its probabilistic estimation. The DeepAR model also encapsulates the seasonal pattern for the post-intervention data and recovers the forecast distribution better than the TBATS (Figure 6b) model, which justifies the values reported in probabilistic error metrics of the models in Table I.

The evidence of DeepAR's good performance on capturing seasonality is demonstrated in Figure 6a, where the weekend distributions of March 21st and 22nd 2020, are forecasted better by the model. The TBATS model, on the other hand, failed to capture these details, and the forecast with a wider prediction interval rendered the model insignificant (left of Figure 6b). Compared to the quantile analysis of the pre-intervention data, the TBATS counterfactual forecast distribution was unable to recover the true observed distribution (Figure 7), whereas the DeepAR model performed good enough to achieve a similar shape of the distribution. Finally, contrasting the DeepAR effect estimation of Italy in the right graph of Figure 6a with the observed values in Figure 5 reveals that there was probably another external factor that affected the upper quantile of the observed distribution beyond the pandemic restrictions.

Table II shows the Average Treatment Effect (ATE) of the impact of Covid-19 on electricity demand in European countries using the DeepAR model, along with their demand change in percentage (a positive value indicates an increase in demand, while a negative value indicates a decrease in demand). Counterfactual probabilistic distribution estimation

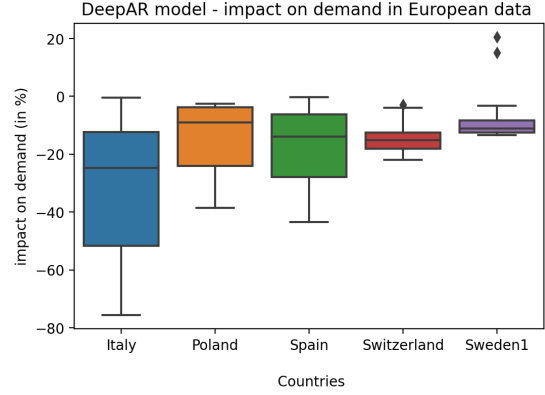


Fig. 8. Boxplot representation of impact of Covid-19 on energy demand in European dataset.

allows for the analysis of effects by quantile, rather than just the median effects as in point forecast estimation. There is a greater impact showing a significant decrease in demand in the troughs of the distribution in Spain and Poland, whereas there is a massive reduction in consumption in Italy from the troughs to the 75th percentile of the distribution. Whereas the impact of Covid-19 on Sweden1 is low in comparison to other countries, as evidenced by Figure 8.

Finally, hypothesis testing was performed to ensure the treatment's relevant effect and the null effect on the control unit. We can confirm significant effects for all treated units and that these effects are statistically different from those of the control unit once both tests returned very low p-values of 4.7e-07, as shown in the last line of Table II. Although the control unit presented a not-so-high p-value of 0.00527, we can conclude an almost null effect for Sweden1.

B. Australian Data

Figure 9 depicts the observed data from NSW, QLD, and TAS in the form of a quantile distribution of the data before and after lockdown intervention to examine the likely concentration of the pandemic effect in the distribution of electricity demand. Given the degree of state restriction, the intervention effect in Tasmania is low and less than in the other states.

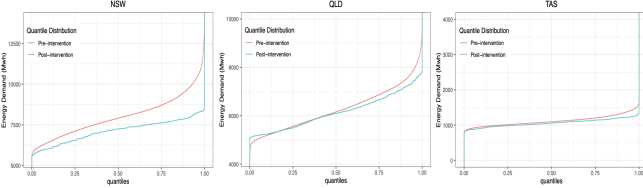


Fig. 9. Quantile distribution of observed pre- and post-intervention data of NSW, QLD and TAS.

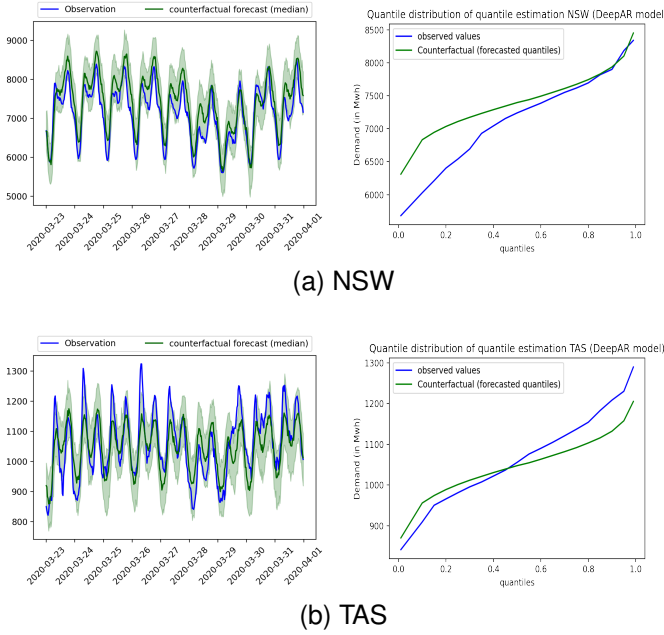


Fig. 10. Point counterfactual forecast with 10% and 90% prediction confidence interval (left) and the quantile distribution of the counterfactual forecast (right) of the DeepAR model.

Hence, such as in the European case, we start by verifying the results for the control units (Tasmania) in the Australian energy use case which are shown in Table III. We see that here, the DeepAR model outperformed all benchmark models. Along with the better distribution recovery ability, the model surpassed all models in analysing the median point forecasting errors. After the DeepAR model, the TBATS model is adequate for point forecasting, whereas the probabilistic error metric of the RNN model is comparable to DeepAR in predicting probabilistic forecasts.

TABLE III
ERROR METRIC RESULTS FOR THE CONTROL UNIT (TASMANIA) OF THE AUSTRALIAN DATASET.

Method	WAPE	WRMSPE	MSIS	CRPS
DeepAR	0.050	0.061	6.765	0.045
RNN	0.084	0.108	9.634	0.060
FFNN	0.765	1.355	186.305	0.694
Seasonal Naïve	0.113	0.130	61.771	0.096
ETS	0.204	0.241	100.856	0.381
TBATS	0.088	0.103	26.494	0.098

Moving on to the analysis of the Australian treated states, we focus our analysis on the DeepAR results, considering it is the best performing method in the previous baseline control

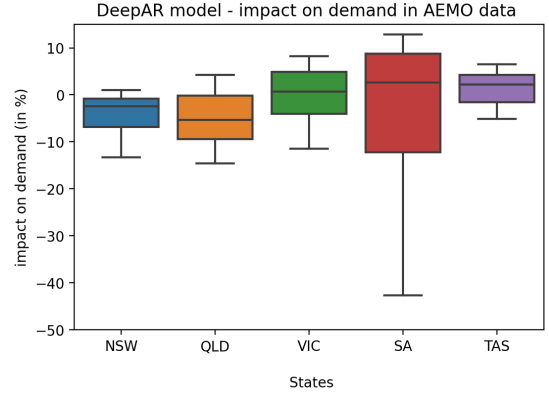


Fig. 11. Boxplot representation of impact of Covid-19 on energy demand in Australian dataset.

error discussion. The DeepAR point forecasting for NSW (left of Figure 10a) shows that the peak observed in the daily distribution of the intervention period falls within the model's prediction confidence interval, demonstrating a small impact during the maximum periods of consumption. On the other hand, the model's result shows a considerable reduction in the lower quantiles demand. Both effects are demonstrated by the right plot of Figure 10a, which displays the estimated counterfactual quantile distribution. In the case of Tasmania (control unit), the observed data peak is outside the prediction confidence interval (left of Figure 10b), and the control unit demonstrates a slight positive effect over the demand peaks, which might be due to a warm weather period as Tasmania did not impose lockdowns, and had no Covid-19 cases at the time, so that large behaviour changes in the population seem unlikely.

Table IV shows the ATE of the DeepAR model for each quantile of the forecasted counterfactual distribution and the percentage change in demand with respect to the observed data. It can be seen that there is a reduction in demand for NSW throughout the entire forecasted probability distribution, whereas for the other states, the demand reduction is only observed in the troughs, and the demand in peak hours contrarily increases. Interestingly, we can see an almost null effect in the median of the electricity consumption distribution in Victoria and South Australia after the lockdown (0.09% and 2.04% of change, respectively); however, the distribution changes completely, with higher peaks of consumption and lower troughs after the restriction measures. Each state's impact caused by Covid-19 is illustrated in the boxplot in Figure 11.

The p-values of NSW and QLD (Table IV) confirm relevant ATE and that these effects are different in terms of statistical significance from those observed in the control unit, respectively. However, the results for VIC and SA do not have a significance to confidently classify them as treated or confirm that the effects come from the lockdown restrictions. They are also not statistically different from TAS. These results lead us to conclude that the lower changes observed in VIC and SA could be also related to other factors (such as weather) than the lockdown. On the other hand, the test confirms the null

TABLE IV
AVERAGE CAUSAL EFFECT AND CHANGE IN ENERGY CONSUMPTION FOR THE AUSTRALIAN DATASET USING THE DEEPAR MODEL.

Quantiles	New South Wales		Queensland		Victoria		South Australia		Tasmania	
	Avg. Causal Effect(in Mwh)	Change in Demand (%)	Avg. Causal Effect(in Mwh)	Change in Demand (%)	Avg. Causal Effect(in Mwh)	Change in Demand (%)	Avg. Causal Effect(in Mwh)	Change in Demand (%)	Avg. Causal Effect(in Mwh)	Change in Demand (%)
0.1	-804.57	-13.35	-749.85	-14.30	-348.77	-9.21	-320.17	-42.63	-46.57	-5.12
0.25	-569.54	-8.71	-732.57	-13.30	-188.36	-4.57	-136.65	-13.87	-20.09	-2.05
0.3	-480.59	-7.18	-662.14	-11.75	-100.36	-2.36	-78.18	-7.41	-16.31	-1.64
0.4	-246.17	-3.50	-495.75	-8.40	-36.17	-0.82	-21.69	-1.92	-8.52	-0.83
0.5	-156.86	-2.17	-406.43	-6.67	3.84	0.09	24.41	2.04	8.12	0.77
0.6	-106.60	-1.44	-306.64	-4.89	79.60	1.72	61.37	4.91	26.76	2.45
0.75	-56.36	-0.78	-85.50	-1.28	256.59	5.22	112.10	8.42	45.18	3.97
0.8	-48.95	-0.64	19.74	0.29	328.63	6.53	136.33	9.96	50.81	4.40
0.95	82.41	1.01	314.47	4.23	442.51	8.25	191.02	12.85	72.38	5.88
0.99	-111.19	-1.33	280.7	3.64	332.81	6.10	171.77	11.27	84.36	6.54
p-values	$6.7e-06 / 0.00025$		$0.001 / 0.00025$		$0.87 / 0.66$		$0.87 / 0.78$		0.06	

effect over TAS with a p-value of 0.06.

This information can be used by a smart grid operator and generator/distributor to identify the actual and precise uncertainty in electricity demand. During policy interventions, this approach allows policymakers to make critical decisions in the smart grid environment, such as grid planning, voltage regulation, and accurate load/price forecasting once the analysis provides us with the effects of each quantile. The impact of policy implementation can be determined at the quantile level of the distribution, and as a result, policy decisions or policy amendments can be made accordingly. Using our framework, the counterfactual approach for causal effect analysis under the more complex and non-uniform intervention impacts leads to an analysis of the intervention's behaviour on our target variable.

VI. CONCLUSION

Grid balancing under uncertainty is critical in smart grids. While ensuring power grid balance, one of the major issues in demand response programs is responding to external interventions that cause grid instability. Here, it is essential to investigate how the interventions affect the distribution of energy profiles. The proposed framework models the conditional quantile functions to build counterfactual distribution outcomes and estimate the distributional effect caused by non-uniform interventions.

To the best of our knowledge, no work in the electricity literature has used a probabilistic forecasting model with GFMs to evaluate the uncertainty in demand/price affected by any intervention. Many previous works have, however, estimated the overall percentage change in demand due to Covid-19, but without taking a probabilistic approach to analyse the effect of Covid-19 on the electricity industry.

The presented work proposes a global RNN-based probabilistic forecasting modelling framework to fill the gap and provides insights to policymakers to make the right decision during treatment uncertainty in the target variable. Causal impact analysis becomes more difficult in the presence of a non-uniform pattern of impact or data with skewness and heavy tails. Our framework's causal effect estimation of demand provides energy sector managers with insights for grid

planning, load/voltage optimisation, and load forecasting in uncertainty.

Some limitations of our approach that could be addressed in future work include the fact that we currently do not use the optimisation of model hyperparameters. Other external predictors which are known to highly influence the energy demand (e.g., the weather), can be inputted into the model to improve model accuracy. Our work can be expanded to analyse different types of electricity markets like residential, non-residential, commercial, and others. Our probabilistic GFM-RNN-based framework for counterfactual prediction has demonstrated the efficacy of learning a global model from nonlinear, unrelated time series at various scales and mapping complex patterns.

ACKNOWLEDGMENTS

This research was supported by the Australian Research Council under grant DE190100045, Monash University Graduate Research funding and MASSIVE - High performance computing facility, Australia.

REFERENCES

- [1] D. Arize and T. N. Rios, "A comparison study on time series forecasting given smart grid load uncertainties," in *2019 8th Brazilian Conference on Intelligent Systems (BRACIS)*. IEEE, 2019, pp. 257–262.
- [2] A. Abada, M. St-Hilaire, and W. Shi, "Auction-based scheduling of excess energy consumption to enhance grid upward flexibility," *IEEE Access*, vol. 10, pp. 5944–5956, 2021.
- [3] T. T. Kim and H. V. Poor, "Scheduling power consumption with price uncertainty," *IEEE Transactions on Smart Grid*, vol. 2, no. 3, pp. 519–527, 2011.
- [4] T. Hong, J. Xie, and J. Black, "Global energy forecasting competition 2017: Hierarchical probabilistic load forecasting," *International Journal of Forecasting*, vol. 35, no. 4, pp. 1389–1399, 2019.
- [5] T. Hong, P. Pinson, S. Fan, H. Zareipour, A. Troccoli, and R. J. Hyndman, "Probabilistic energy forecasting: Global energy forecasting competition 2014 and beyond,"

International Journal of forecasting, vol. 32, no. 3, pp. 896–913, 2016.

[6] D. Salinas, V. Flunkert, J. Gasthaus, and T. Januschowski, “DeepAR: Probabilistic forecasting with autoregressive recurrent networks,” *International Journal of Forecasting*, vol. 36, no. 3, pp. 1181–1191, 2020.

[7] G. Dudek, P. Pełka, and S. Smyl, “A hybrid residual dilated LSTM and exponential smoothing model for midterm electric load forecasting,” *IEEE Transactions on Neural Networks and Learning Systems*, vol. 33, no. 7, pp. 2879–2891, 2022.

[8] G. I. Nagy, G. Barta, S. Kazi, G. Borbély, and G. Simon, “GEFCom2014: Probabilistic solar and wind power forecasting using a generalized additive tree ensemble approach,” *International Journal of Forecasting*, vol. 32, no. 3, pp. 1087–1093, 2016.

[9] International Energy Agency. [Online]. Available: <https://www.iea.org/topics/net-zero-emissions>

[10] Z. Zhang, R. Li, and F. Li, “A novel peer-to-peer local electricity market for joint trading of energy and uncertainty,” *IEEE Transactions on Smart Grid*, vol. 11, no. 2, pp. 1205–1215, 2019.

[11] P. Samadi, H. Mohsenian-Rad, V. W. Wong, and R. Schober, “Tackling the load uncertainty challenges for energy consumption scheduling in smart grid,” *IEEE Transactions on Smart Grid*, vol. 4, no. 2, pp. 1007–1016, 2013.

[12] A. J. Conejo, J. M. Morales, and L. Baringo, “Real-time demand response model,” *IEEE Transactions on Smart Grid*, vol. 1, no. 3, pp. 236–242, 2010.

[13] E. Buechler, S. Powell, T. Sun, C. Zanocco, N. Astier, J. Bolorinos, J. Flora, H. Boudet, and R. Rajagopal, “Power and the pandemic: Exploring global changes in electricity demand during Covid-19,” *arXiv preprint arXiv:2008.06988*, 2020.

[14] A. Rybak and A. Rybak, “The impact of the Covid-19 pandemic on gaseous and solid air pollutants concentrations and emissions in the EU, with particular emphasis on Poland,” *Energies*, vol. 14, no. 11, p. 3264, 2021.

[15] K. Bandara, C. Bergmeir, and S. Smyl, “Forecasting across time series databases using recurrent neural networks on groups of similar series: A clustering approach,” *Expert Systems with Applications*, vol. 140, p. 112896, 2020.

[16] R. Wen, K. Torkkola, B. Narayanaswamy, and D. Madeka, “A Multi-Horizon quantile recurrent forecaster,” in *Neural Information Processing Systems*, Nov. 2017.

[17] S. Smyl, “A hybrid method of exponential smoothing and recurrent neural networks for time series forecasting,” *International Journal of Forecasting*, vol. 36, no. 1, pp. 75–85, 2020.

[18] S. Makridakis, E. Spiliotis, and V. Assimakopoulos, “M5 accuracy competition: Results, findings, and conclusions,” *International Journal of Forecasting*, 2022.

[19] T. Januschowski, J. Gasthaus, Y. Wang, D. Salinas, V. Flunkert, M. Bohlke-Schneider, and L. Callot, “Criteria for classifying forecasting methods,” *International Journal of Forecasting*, vol. 36, no. 1, pp. 167–177, 2020. [Online]. Available: <https://doi.org/10.1016/j.ijforecast.2019.05.008>

[20] H. Hewamalage, C. Bergmeir, and K. Bandara, “Global models for time series forecasting: A simulation study,” *Pattern Recognition*, vol. 124, p. 108441, 2022.

[21] P. Montero-Manso and R. J. Hyndman, “Principles and algorithms for forecasting groups of time series: Locality and globality,” *International Journal of Forecasting*, vol. 37, no. 4, pp. 1632–1653, 2021.

[22] P. Grecov, K. Bandara, C. Bergmeir, K. Ackermann, S. Campbell, D. Scott, and D. Lubman, “Causal inference using global forecasting models for counterfactual prediction,” in *Pacific-Asia Conference on Knowledge Discovery and Data Mining*. Springer, 2021, pp. 282–294.

[23] P. Grecov, A. N. Prasanna, K. Ackermann, S. Campbell, D. Scott, D. I. Lubman, and C. Bergmeir, “Probabilistic causal effect estimation with global neural network forecasting models,” *IEEE Transactions on Neural Networks and Learning Systems*, pp. 1–15, 2022.

[24] A. S. Kwekha-Rashid, H. N. Abduljabbar, and B. Alhayani, “Coronavirus Disease (Covid-19) cases analysis using machine-learning applications,” *Applied Nanoscience*, pp. 1–13, 2021.

[25] B. Janzen and D. Radulescu, “Electricity use as a real-time indicator of the economic burden of the Covid-19-related lockdown: Evidence from Switzerland,” *CESifo Economic Studies*, vol. 66, no. 4, pp. 303–321, 2020.

[26] J. Bedi and D. Toshniwal, “Deep learning framework to forecast electricity demand,” *Applied energy*, vol. 238, pp. 1312–1326, 2019.

[27] D. W. Van der Meer, M. Shepero, A. Svensson, J. Widén, and J. Munkhammar, “Probabilistic forecasting of electricity consumption, photovoltaic power generation and net demand of an individual building using Gaussian processes,” *Applied energy*, vol. 213, pp. 195–207, 2018.

[28] A. Liu, W. Miller, J. Chiou, S. Zedan, T. Yigitcanlar, and Y. Ding, “Aged Care energy use and peak demand change in the Covid-19 year: Empirical evidence from Australia,” *Buildings*, vol. 11, no. 12, p. 570, 2021.

[29] J. Abrell, M. Kosch, and S. Rausch, “How effective is carbon pricing?—A machine learning approach to policy evaluation,” *Journal of Environmental Economics and Management*, vol. 112, p. 102589, 2022.

[30] C. Graf, F. Quaglia, and F. A. Wolak, “(Machine) learning from the Covid-19 lockdown about electricity market performance with a large share of renewables,” *Journal of Environmental Economics and Management*, vol. 105, p. 102398, 2021.

[31] S. García, A. Parejo, E. Personal, J. I. Guerrero, F. Biscarri, and C. León, “A retrospective analysis of the impact of the Covid-19 restrictions on energy consumption at a disaggregated level,” *Applied energy*, vol. 287, p. 116547, 2021.

[32] F. Burlig, C. Knittel, D. Rapson, M. Reguant, and C. Wolfram, “Machine learning from schools about energy efficiency,” *Journal of the Association of Environ-*

mental and Resource Economists, vol. 7, no. 6, pp. 1181–1217, 2020.

[33] M. J. Beck and D. A. Hensher, “Australia 6 months after Covid-19 restrictions part-1: Changes to travel activity and attitude to measures,” *Transport Policy*, 2021.

[34] S. PERCY and B. Mountain, “Covid-19 and social distancing: Does it show up in the demand for electricity?” *Victoria*, vol. 42, no. 40, p. 41, 2020.

[35] E. Bompard, C. Mosca, P. Colella, G. Antonopoulos, G. Fulli, M. Masera, M. Poncela-Blanco, and S. Vitiello, “The immediate impacts of Covid-19 on European electricity systems: A first assessment and lessons learned,” *Energies*, vol. 14, no. 1, p. 96, 2020.

[36] E. J. Orlowski and D. J. Goldsmith, “Four months into the Covid-19 pandemic, Sweden’s prized herd immunity is nowhere in sight,” *Journal of the Royal Society of Medicine*, vol. 113, no. 8, pp. 292–298, 2020.

[37] M. Czosnyka, B. Wnukowska, and K. Karbowa, “Electrical energy consumption and the energy market in Poland during the Covid-19 pandemic,” in *2020 Progress in Applied Electrical Engineering (PAEE)*. IEEE, 2020, pp. 1–5.

[38] S. Nikkhah, A. Allahham, M. Royapoor, J. W. Bialek, and D. Giaouris, “Optimising building-to-building and building-for-grid services under uncertainty: A robust rolling horizon approach,” *IEEE Transactions on Smart Grid*, vol. 13, no. 2, pp. 1453–1467, 2021.

[39] A. Bortolato, P. Faria, and Z. Vale, “Probabilistic determination of consumers response and consumption management strategies in demand response programs,” in *2020 IEEE/PES Transmission and Distribution Conference and Exposition (T&D)*. IEEE, 2020, pp. 1–5.

[40] J. M. Lujano-Rojas, G. Osório, R. Dufo-Lopez, J. L. Bernal-Agustín, M. Shafie-Khah, and J. P. Catalão, “Probabilistic modeling of smart residential energy systems,” in *2017 IEEE PES Innovative Smart Grid Technologies Conference Europe (ISGT-Europe)*. IEEE, 2017, pp. 1–6.

[41] S. B. Taieb, R. Huser, R. J. Hyndman, and M. G. Genton, “Forecasting uncertainty in electricity smart meter data by boosting additive quantile regression,” *IEEE Transactions on Smart Grid*, vol. 7, no. 5, pp. 2448–2455, 2016.

[42] N. Doudchenko and G. W. Imbens, “Balancing, regression, difference-in-differences and synthetic control methods: A synthesis,” National Bureau of Economic Research, Tech. Rep., 2016.

[43] A. Abadie, A. Diamond, and J. Hainmueller, “Synthetic control methods for comparative case studies: Estimating the effect of California’s tobacco control program,” *Journal of the American Statistical Association*, vol. 105, no. 490, pp. 493–505, 2010.

[44] C. Carvalho, R. Masini, and M. C. Medeiros, “Arco: an artificial counterfactual approach for high-dimensional panel time-series data,” *Journal of Econometrics*, vol. 207, no. 2, pp. 352–380, 2018.

[45] K. H. Brodersen, F. Gallusser, J. Koehler, N. Remy, and S. L. Scott, “Inferring causal impact using Bayesian structural time-series models,” *The Annals of Applied Statistics*, vol. 9, no. 1, pp. 247–274, 2015.

[46] D. B. Rubin, “Estimating causal effects of treatments in randomized and non-randomized studies,” *Journal of educational Psychology*, vol. 66, no. 5, p. 688, 1974.

[47] A. Alexandrov, K. Benidis, M. Bohlke-Schneider, V. Flunkert, J. Gasthaus, T. Januschowski, D. C. Maddix, S. S. Rangapuram, D. Salinas, J. Schulz *et al.*, “Gluonts: Probabilistic and neural time series modeling in Python.” *J. Mach. Learn. Res.*, vol. 21, no. 116, pp. 1–6, 2020.

[48] Australian Energy Market Operator(AEMO). [Online]. Available: <https://aemo.com.au/>

[49] ENTSO-E transparency platform. [Online]. Available: <https://transparency.entsoe.eu/>

[50] R. Hyndman, A. B. Koehler, J. K. Ord, and R. D. Snyder, *Forecasting with exponential smoothing: the state space approach*. Springer Science & Business Media, 2008.

[51] A. M. De Livera, R. J. Hyndman, and R. D. Snyder, “Forecasting time series with complex seasonal patterns using exponential smoothing,” *Journal of the American statistical association*, vol. 106, no. 496, pp. 1513–1527, 2011.

[52] H. Hewamalage, K. Ackermann, and C. Bergmeir, “Forecast evaluation for data scientists: Common pitfalls and best practices,” *arXiv preprint arXiv:2203.10716*, 2022.

[53] P. Virtanen, R. Gommers, T. E. Oliphant, M. Haberland, T. Reddy, D. Cournapeau, E. Burovski, P. Peterson, W. Weckesser, J. Bright, S. J. van der Walt, M. Brett, J. Wilson, K. J. Millman, N. Mayorov, A. R. J. Nelson, E. Jones, R. Kern, E. Larson, C. J. Carey, İ. Polat, Y. Feng, E. W. Moore, J. VanderPlas, D. Laxalde, J. Perktold, R. Cimrman, I. Henriksen, E. A. Quintero, C. R. Harris, A. M. Archibald, A. H. Ribeiro, F. Pedregosa, P. van Mulbregt, and SciPy 1.0 Contributors, “SciPy 1.0: Fundamental algorithms for scientific computing in Python,” *Nature Methods*, vol. 17, pp. 261–272, 2020.

BIOGRAPHY

Ankitha Nandipura Prasanna received the Bachelor of Engineering in Computer Science and Engineering from the Visvesvaraya Technological University, India, in 2014. She finished her Master degree in Artificial Intelligence at the Faculty of Information Technology, Monash University, Melbourne, Australia in 2022. Her research interests includes deep neural networks and time series forecasting.

Priscila Grecov is a PhD student in Computer Science at the Faculty of Information Technology, Monash University, Melbourne, Australia. Her research interests include Causal Inference, Deep Neural Networks and time series forecasting using Machine Learning methods. She finished her Master degree in Data Science at Monash university in 2020, and also holds an M.Sc. degree in Mathematics from the Institute of Pure and Applied Mathematics, Brazil. Her B.Sc. degree is in Economics obtained from the University of Brasilia, Brazil.

Angela Dieyu Weng is a Year 12 IB student at Lauriston Girls’ School, Melbourne, Australia. Her research interests include applied and computational mathematics and machine learning. Angela has studied university-level mathematics courses at her leisure. She is planning to pursue a degree in the field of computational mathematics at university.

Christoph Bergmeir is a Senior Research Fellow in Data Science and Artificial Intelligence, and a 2019 ARC DECRA Fellow in the Department of Data Science and Artificial Intelligence at Monash University. His fellowship is on the development of “efficient and effective analytics for real-world time series forecasting”. Christoph holds a PhD in Computer Science from the University of Granada, Spain, and an M.Sc. degree in Computer Science from the University of Ulm, Germany.

APPENDIX

ADDITIONAL FIGURES

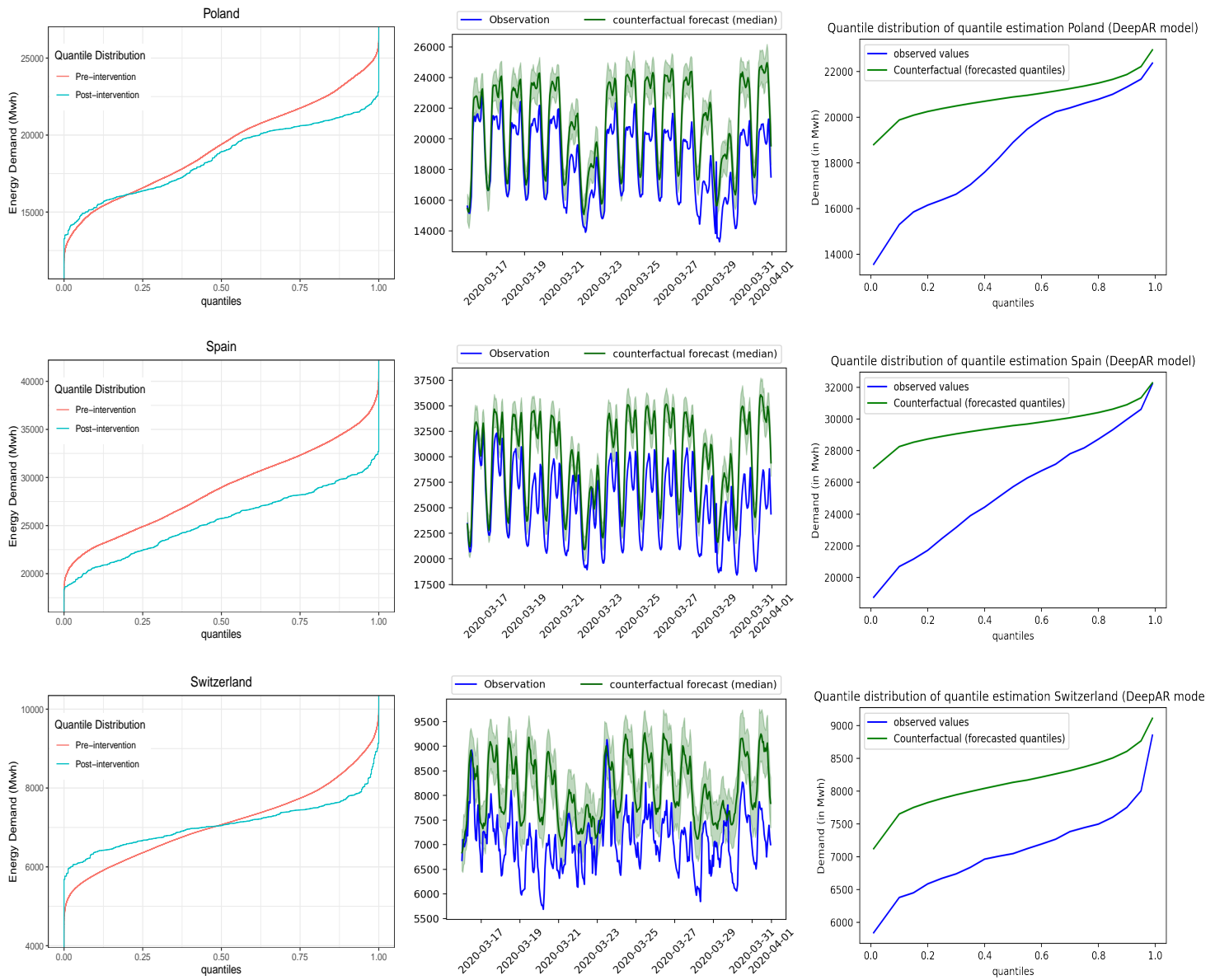


Fig. 12. European data – Observed quantile distribution of pre- and post-intervention data (left), DeepAR model's forecast (middle) and its forecast quantile distribution (right).

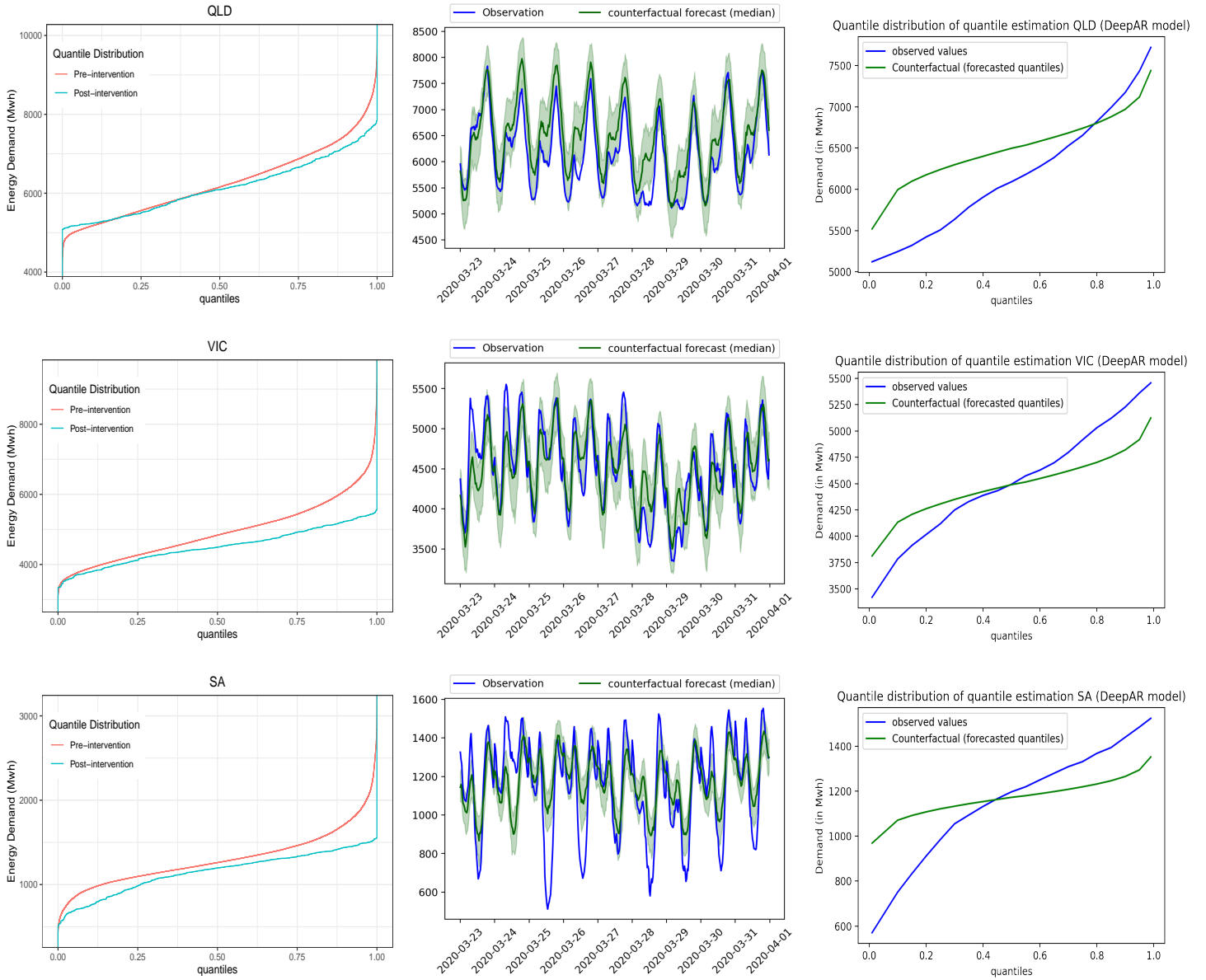


Fig. 13. Australian data – Observed quantile distribution of pre- and post-intervention data (left), DeepAR model's forecast (middle) and its forecast quantile distribution (right).